Functionalized Polymeric Membrane with Enhanced Mechanical and Biological Properties to Control the Degradation of Magnesium Alloy

Hoi Man Wong, Ying Zhao, Frankie K. L. Leung, Tingfei Xi, Zhixiong Zhang, Yufeng Zheng, Shuilin Wu, Keith D. K. Luk, Kenneth M. C. Cheung, Paul K. Chu, and Kelvin W. K. Yeung**

To achieve enhanced biological response and controlled degradation of magnesium alloy, a modified biodegradable polymer coating called polycaprolactone (PCL) is fabricated by a thermal approach in which the heat treatment neither alters the chemical composition of the PCL membrane nor the rate of magnesium ion release, pH value, or weight loss, compared with the untreated sample. The changes in the crystallinity, hydrophilicity, and oxygen content of heat-treated PCL coating not only improve the mechanical adhesion strength between the coating and magnesium substrate but also enhance the biological properties. Moreover, the thermally modified sample can lead to higher spreading and elongation of osteoblasts, due to the enhanced hydrophilicity and C=O to C—O functional group ratio. In the analyses of microcomputed tomography from one to four weeks postoperation, the total volume of new bone formation on the heat-treated sample is 10%–35% and 70%–90% higher than that of the untreated and uncoated controls, respectively. Surprisingly, the indentation modulus of the newly formed bone adjacent to the heat-treated sample is ≈20% higher than that of both controls. These promising results reveal the clinical potential of the modified PCL coating on magnesium alloy in orthopedic applications.

1. Introduction

Biometals, such as medical-grade titanium alloys and stainless steel, are commonly used in orthopedic implants.[1,2] However, besides the foreign body effect, these nondegradable metallic materials may induce stress shielding effects after implantation, due to the mismatch in the mechanical properties between the metals and human bones.[3] When stress shielding occurs, the interface between the implant and tissues becomes unstable, and revision surgery may be necessary.

Biodegradable polymers, such as poly(glycolic acid) (PLGA) and poly(lactic acid) (PLA), are the other types of commonly used biodegradable materials,[4,5] but their mechanical properties are not adequate in some load-bearing situations.[6] For instance, Litsky[7] reported that a second surgical procedure was needed, due to the failure of the fixation

Dr. H. M. Wong, Dr. Y. Zhao, Prof. F. K. L. Leung, Prof. K. D. K. Luk, Prof. K. M. C. Cheung, Dr. K. W. K. Yeung
Department of Orthopaedics and Traumatology
The University of Hong Kong
Pokfulam, Hong Kong, China
E-mail: wkkyeung@hku.hk

Dr. Y. Zhao, Prof. P. K. Chu
Department of Physics and Materials Science
City University of Hong Kong
Tat Chee Avenue, Kowloon, Hong Kong, China
E-mail: paul.chu@cityu.edu.hk

Dr. Y. Zhao
Center for Human Tissues and Organs Degeneration
Shenzhen Institutes of Advanced Technology
Chinese Academy of Sciences
Shenzhen 518055, China

Prof. F. K. L. Leung, Dr. K. W. K. Yeung
Shenzhen Key Laboratory for Innovative Technology in Orthopaedic Trauma
The University of Hong Kong Shenzhen Hospital
1 Haiyuan 1st Road, Futian District, Shenzhen 518000, China

Prof. T. Xi, Dr. Z. Zhang, Prof. Y. Zheng
Center for Biomedical Materials and Tissue Engineering
Academy for Advanced Interdisciplinary Studies
Peking University
Beijing 100871, China

Prof. S. Wu
Hubei Collaborative Innovation Center for Advanced Organic Chemical Materials
Ministry of Education Key Laboratory for the Green Preparation and Application of Functional Materials
Hubei Province Key Laboratory of Industrial Biotechnology
Faculty of Materials Science and Engineering
Hubei University
430000 Wuhan, China

DOI: 10.1002/adhm.201601269

implants made of biodegradable polymers. Hence, degradable biomaterials with sufficient mechanical properties are needed. Biodegradable magnesium alloys possessing more "bone-like" mechanical properties have been investigated as alternatives in orthopedic applications, such as fracture fixation.[8,9]

Magnesium-based materials were first introduced to orthopedic and trauma surgery in the 19th century,[10,11] but progress was stifled, due to rapid degradation and uncontrolled release of hydrogen gas in the physiological environment.[12–15] To overcome these shortcomings, methods such as surface treatment[16,17] and alloying[18] have been explored. For surface treatment, coating with polymers, such as polycaprolactone (PCL) and poly(lactic acid) (PLA), are two of the most commonly used coating materials.[19,20] However, the intrinsic hydrophobicity of the polymers does not favor adhesion or proliferation of osteoblasts, thereby adversely affecting bone-to-implant integration.[21] Furthermore, the absence of charged groups and the lack of bioactive functional groups tend to inhibit cell attachment and proliferation.[21–23] Consequently, plasma treatment,[24] protein deposition,[25] chemical treatment,[26] and block copolymerization[27] have been investigated to enhance the chemical and biological functions. In addition to the biological characteristics, physical adhesion between the polymer membrane and metal substrate is another concern in clinical use, since insufficient adhesion force results in membrane delamination when subjected to mechanical shear. Although different types of surface treatments have been applied to alter the surface tension, roughness, and chemistry of metallic substrates to increase the bonding strength at the metal/polymer interface,[28–30] the intrinsic hydrophobic property of the polymer coating is still unsolved. Herein, a custom-made heat treatment process has been adopted to functionalize the biological features of PCL coating in order to favor the adhesion and proliferation of osteoblasts as well as in vivo bone formation. This process can also help enhance coating–substrate adhesion.

2. Results

2.1. Characterization

2.1.1. Thickness

Figure 1 shows the thickness of the PCL membrane. The thickness of the PCL membrane is ≈30 µm.

2.1.2. Crystallinity

Table 1 shows the melting temperature (T_m), the change of melting of heat (ΔH_m), and the crystallinity degree X_c% of the untreated and heat-treated polymer membrane. The melting point decreased from 57.29 to 56.8 °C after heat treatment, whereas the crystallinity increased by ≈4%. This shows that the heat treatment process is able to enhance the crystallization of PCL membrane.

Table 1. Thermal properties of untreated and heat-treated PCL membrane by differential scanning calorimetry.

Sample	T_m [°C]	ΔH_m [J g^{-1}]	X_c [%]
Untreated PCL membrane	57.29	53.98	38.8
Heat-treated PCL membrane	56.80	59.39	42.7

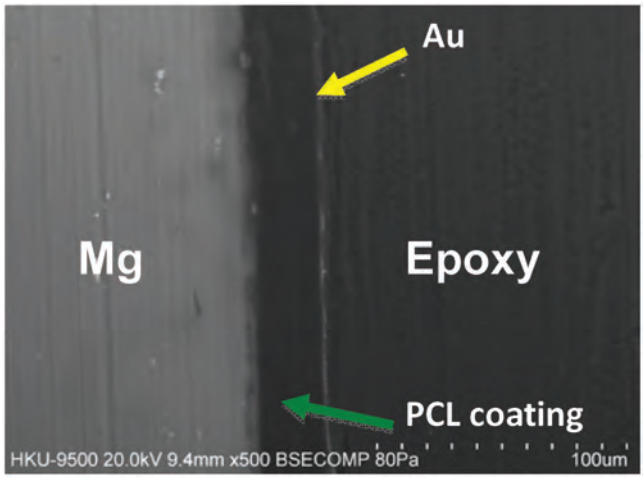

Figure 1. SEM picture showing PCL membrane thickness, with the yellow arrow showing the gold coating and green arrow showing the PCL coating. The thickness of the coating is ≈30 µm.

2.1.3. Composition

Figure 2 presents the Fourier transform infrared spectroscopy (FTIR) spectrum of the untreated and heat-treated polymer membrane. The spectrums show peak at around 3500 cm^{-1}, which corresponds to the hydroxyl group. In addition, the PCL-related stretching modes are represented by the peaks at 1727 cm^{-1} (C=O stretching), 2943 cm^{-1} (asymmetric CH_2 stretching), 2866 cm^{-1} (symmetric CH_2 stretching),

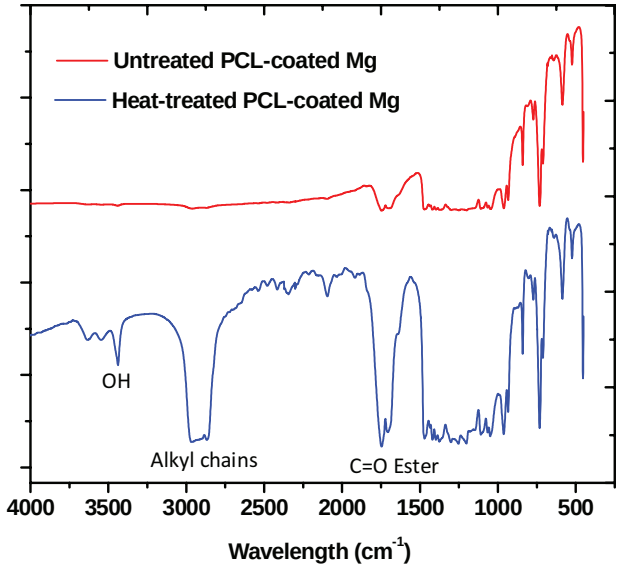

Figure 2. Composition of the untreated and heat-treated PCL membrane.

1294 cm^{-1} (C—O and C—C stretching), 1170 cm^{-1} (symmetric C—O—C stretching), and 1240 cm^{-1} (asymmetric C—O—C stretching).[31–33] All of the related peaks are identified from both the untreated and heat-treated PCL samples, suggesting that no additional functional groups are found on the PCL membrane after annealing. However, the peak intensities from the heat-treated samples are higher than the untreated samples.

2.1.4. Structural Analysis

The X-ray diffraction (XRD) patterns of the untreated and heat-treated PCL-coated magnesium samples are depicted in **Figure 3**. In addition to the peaks from the magnesium substrate, two diffraction peaks at $2\theta = 21.4°$ and 23.8° are observed for the untreated and heat-treated polymer-coated samples, corresponding to the diffraction of the (110) and (200) planes of semicrystalline PCL, respectively.[34] The intensity of these two diffraction peaks from the heat-treated samples is higher than that from the untreated samples, indicating that annealing enhances crystallization of PCL.

2.1.5. Hydrophilicity

The hydrophilicity of the samples was evaluated by the static sessile drop method with deionized water, and the images of the water droplets are depicted in **Figure 4**. The average water contact angle on the untreated PCL membrane was close to 98°, whereas that on the heat-treated PCL membrane is 77°. The heat-treated PCL membrane is thus more hydrophilic.

2.1.6. Atomic Concentration

Quantitative X-ray photoelectron spectroscopy (XPS) disclosed that the oxygen-to-carbon ratios of the untreated and heat-treated PCL membranes were 30.1% and 31.4%, respectively. The O 1s spectra can be deconvoluted into C=O at 532.1 eV and C—O at 533.4 eV by Gaussian–Lorentzian peak fitting (**Figure 5**). After the heat treatment, the ratio of C=O to C—O increased, and it is believed to be the primary reason for the observed difference in the hydrophilicity and adhesion properties.

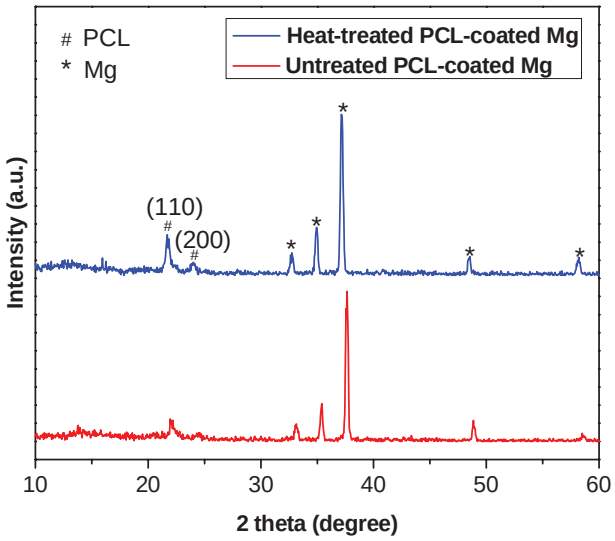

Figure 3. X-ray diffraction (XRD) patterns acquired from the untreated and heat-treated PCL-coated magnesium alloys.

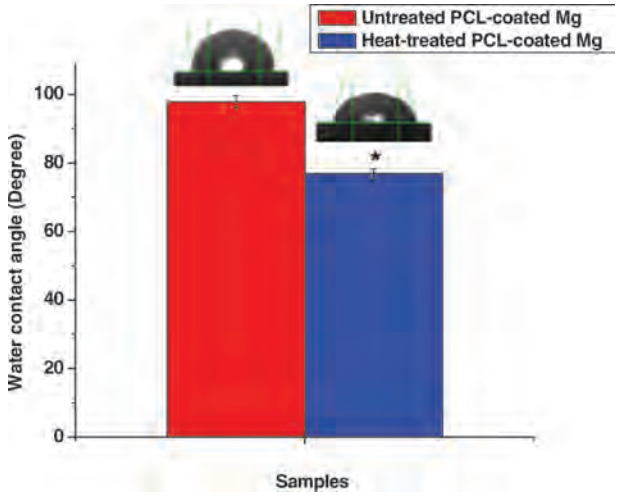

Figure 4. Water contact angles on the samples showing a smaller ($p < 0.05$) contact angle on the PCL-coated magnesium alloy after the heat treatment.

2.1.7. Bonding Strength

Figure 6 shows the bonding strength, based on the modified peel-off test. The adhesion force of the untreated polymer-coated sample was 2.5 N, whereas that of the heat-treated polymer-coated sample was 3.3 N, indicating an increase of about 30% after annealing ($p < 0.05$).

2.2. Electrochemical Properties

The representative electrochemical impedance spectroscopy (EIS) spectra (Nyquist plots) acquired from the uncoated, untreated, and heat-treated PCL-coated samples are presented in **Figure 7**a. The capacitive arc at high frequencies results from charge transfer, and the capacitive arc at medium frequency results from the effects of the surface film. It is obvious that, after heat treatment, the capacitive arcs are evidently enlarged. Moreover, the visible of the inductive arc in the low-frequency region is probably due to the formation, adsorption, and desorption of corrosion products on the surface. It is known that a larger diameter arc represents better corrosion resistance and, hence, both EIS results indicate that heat treatment appreciably improves the corrosion resistance of AZ91 magnesium alloy. Furthermore, scanning electron microscopy (SEM) revealed a number of cracks on the uncoated sample surface, compared to the untreated and heat-treated PCL-coated samples. No sign of corrosion was found on the heat-treated PCL-coated samples (Figure 7b).

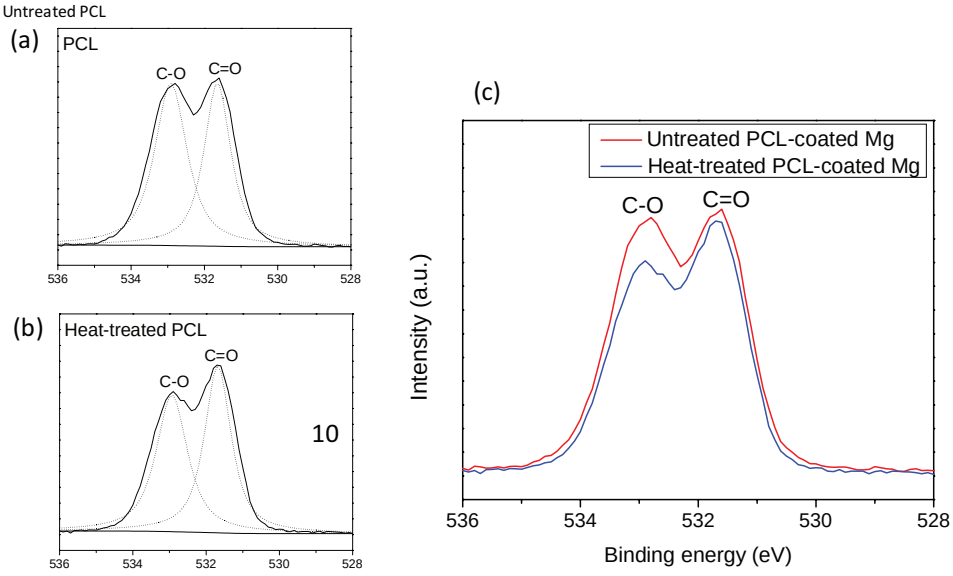

Figure 5. XPS O 1s spectra: a) Untreated and b) heat-treated PCL deposited samples. The dotted lines represent the C—O and C=O spectra deconvoluted from the O 1s spectrum, using the Gaussian–Lorentzian peak fitting model; c) Combined XPS O 1s spectra of the untreated and heat-treated PCL deposited samples. A larger ratio of C=O is observed after the heat treatment.

2.3. Immersion Test

Figure 8a,b shows the Mg ion concentrations and pH. The magnesium ion concentrations determined from the uncoated samples by inductively coupled plasma mass spectrometry (ICP-OES) ranged between 200 ppm on day 1 to 600 ppm on day 14. In comparison, the magnesium ion concentrations released from the untreated and heat-treated PCL-coated sample were below 50 ppm on day 1 and about 150 ppm on day 14. No significant difference was found on the PCL-coated samples before or after heat treatment. The pH of all of the samples increased from day 1 to day 14. After immersion for 1 d, the pH of the uncoated sample increased from 7.4 to 8 and reached 9 on day 14, whereas that of the untreated and heat-treated PCL-coated samples only varied between 7.5 and 7.8 from day 1 to day 14.

Figure 8c shows the weight losses. The weight loss from the uncoated sample increased from 2 mg on day 1 to 7 mg on day 14. In contrast, degradation of the untreated and heat-treated PCL-coated samples was less severe, and the weight loss was ≈1 mg on day 14.

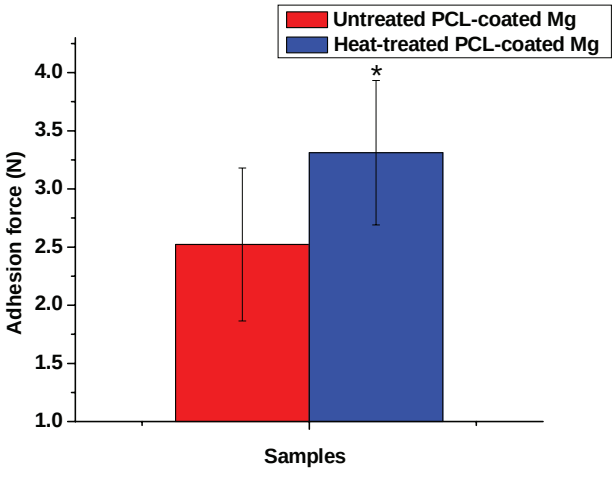

Figure 6. Adhesion force of the untreated and heat-treated PCL-coated magnesium alloys derived from the modified peel-off test.

2.4. Cytocompatibility and Cell Spreading

Figure 9a shows the viable cells on the uncoated, untreated, and heat-treated PCL-coated samples after culturing of enhanced green fluorescent protein osteoblasts (eGFPOB) for 1 and 3 d. In general, the cells were well tolerated on both the untreated and heat-treated PCL-coated samples. The cells on the heat-treated samples were spread well on day 1 and continued to proliferate for 3 d. However, more round-shaped cells were observed on the untreated samples. In contrast, no viable cells were observed from the uncoated sample throughout the culturing period.

The aspect ratio, average cell area, and adhesion cell density after osteoblastic 1 d cell culturing are shown in Figure 9b. The aspect ratio of the cells on the heat-treated polymer-coated sample surface was significantly higher, indicating that the cells were able to elongate. Moreover, ≈20% of cell density was found to be higher on the heat-treated PCL-coated sample as compared to the untreated PCL-coated sample, suggesting that more cells were adhered on the sample surface after heat treatment. Finally, the larger average cell area was found on the heat-treated sample, implying that the surface condition was favorable to cell growth.

2.5. In Vivo Animal Study

2.5.1. Microcomputed (μCT) Tomography

Figure 10a displays the μCT reconstruction images at different time points. Figure 10b,c shows the percentage of new bone formation adjacent to the implant and change in the implant volume, respectively. More than 40% bone resorption was observed from the uncoated sample after one week. In comparison, the volume of adjacent bone formation on the untreated PCL coating increased by 30%, and that on the heat-treated sample went up by 50%. Furthermore, significantly more new bone was observed after one, two, and three weeks from the heat-treated samples than the untreated ones. The bone volume on both the untreated and

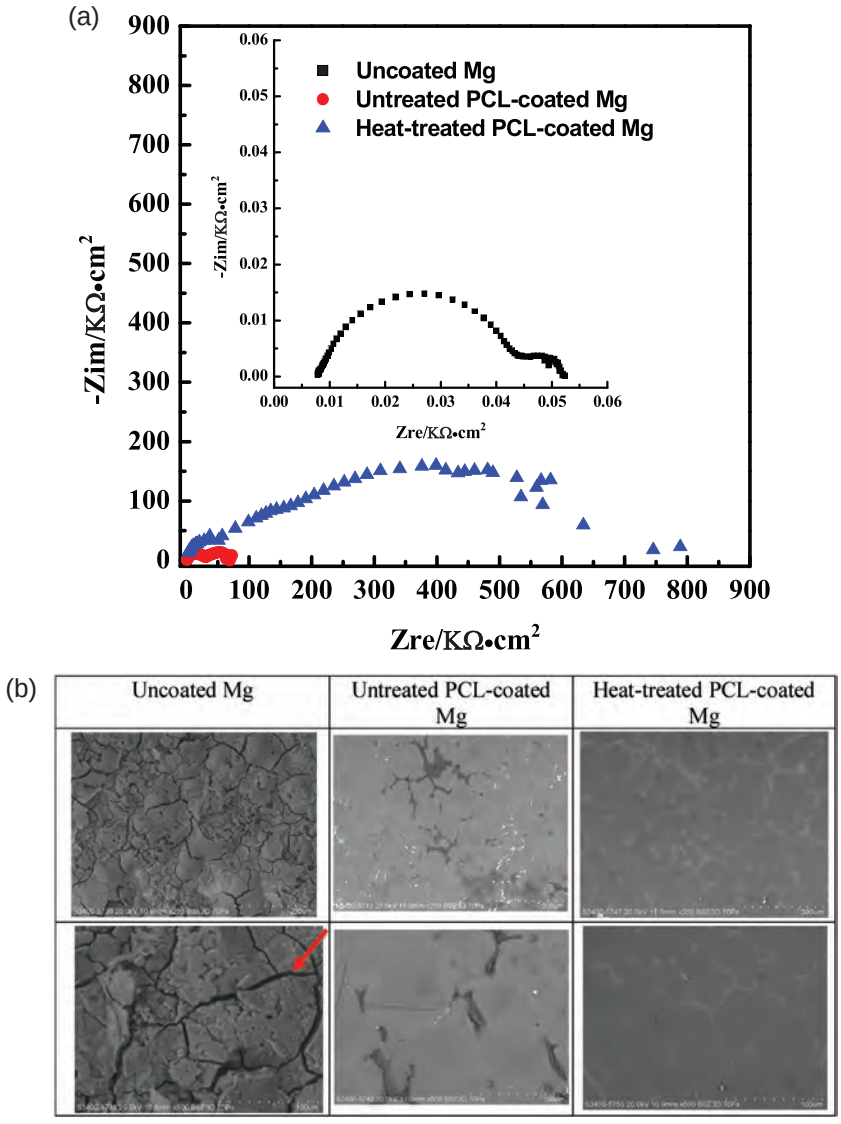

Figure 7. a) EIS spectra of untreated, heat-treated PCL-coated, and uncoated magnesium alloys. b) Surface morphology of the untreated, heat-treated PCL-coated, and uncoated magnesium alloys after electrochemical tests, as revealed by SEM. A large number of cracks (red arrow) are found on the uncoated sample, with little on the untreated sample. No crack is found on the heat-treated PCL-coated sample.

heat-treated samples increased by 60% after eight weeks, and then the rate decreases. With regard to implant degradation, the volume of the untreated and heat-treated samples decreased by ≈2% and 1%, whereas the uncoated sample diminished by 3% after four weeks. The volume of the uncoated sample dropped to below 94% after eight weeks, but that of the coating with and without heat treatment was above 96% and 97%, respectively.

Figure 10d presents the 3D μCT reconstruction images of the newly formed bone on the uncoated, untreated, and heat-treated samples after two months. The uncoated sample showed significantly less volume of new bone formation (0.11 mm^3) than the untreated (3.42 mm^3) and heat-treated (3.64 mm^3) samples.

2.5.2. Magnesium Ion Concentration

Figure 11 shows the percentage changes in the serum magnesium ion concentrations in the rats implanted with the uncoated, untreated, and heat-treated samples, up to eight weeks postoperation. There was no significant difference between preoperation and postoperation.

Figure S1 (Supporting Information) shows the magnesium concentrations in the kidney and liver eight weeks after implantation. The magnesium concentrations in the liver of the animals implanted with the uncoated, untreated, and heat-treated samples were 2, 1.6, and 2.5 ppm g^{-1}, respectively, and those in the kidney were 2.1, 1.8, and 1.9 ppm g^{-1}, respectively. No significant difference was found.

2.5.3. Histological Evaluation

Figure 12 shows the adjacent bone tissue response in the vicinity of the uncoated, untreated, and heat-treated samples after four and eight weeks. New bone formation was observed from both the untreated and heat-treated samples after four and eight weeks, whereas no new bone formation was found on the uncoated sample after four weeks. The presence of fibrous tissue stained in blue in the histological slide is suspected. Although the fibrous tissue disappeared after week 8, there was only a small amount of new bone, compared to the untreated and heat-treated samples.

2.5.4. Mechanical Properties of New Bony Tissues

The modulus of the new bone after four and eight weeks was determined by nanoindentation, as shown in **Figure 13**. The nanoindentation measurements were performed on the bone adjacent to the implants (marked with red crosses) (Figure S2, Supporting Information).

The indentation modulus of the newly formed bone of the heat-treated group could restore to near 80% of the adjacent matured bone, whereas the modulus measurements of the bone formed nearby uncoated and untreated groups were ≈60% only after four and eight weeks of operation. The indentation modulus of the heat-treated sample was 20% higher than that of the uncoated and untreated groups ($p < 0.05$). The material corrosion (marked with blue arrows) was clearly observed from the uncoated sample after eight weeks, as revealed by SEM (Figure S2, Supporting Information). The representative load–displacement curves were shown in Figure S3 (Supporting Information).

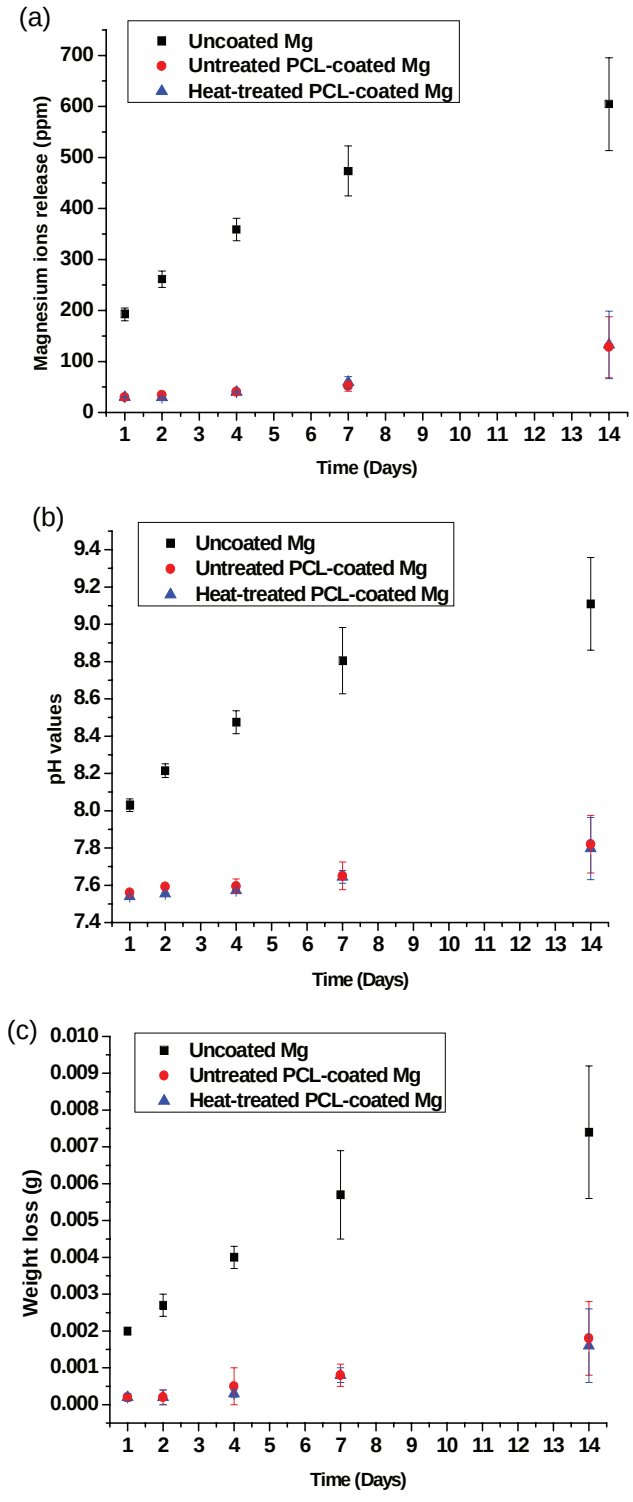

Figure 8. a) Magnesium release from the untreated, heat-treated PCL-coated, and uncoated magnesium alloys with time determined by inductively coupled plasma optical emission spectroscopy (ICP-OES). The values of the untreated and heat-treated samples were found to be significantly different ($p < 0.05$) compared to the uncoated sample. b) pH of the immersion extract from the untreated, heat-treated PCL-coated, and uncoated magnesium alloys with time. All values of both the untreated and heat-treated samples were found to be significantly different ($p < 0.05$), compared to the uncoated sample. c) Weight loss from the untreated, heat-treated PCL-coated, and uncoated magnesium alloys with time. All values of both the untreated and heat-treated samples were found to be significantly different ($p < 0.05$), compared to the uncoated sample.

3. Discussion

Biodegradable magnesium is a potential biometal suitable for bone fracture fixation. However, the degradation rate needs to be controlled carefully to provide adequate mechanical support at the time of bone healing.[9,35] In addition to the aspect of mechanical properties, biological compliance is another major concern, as a large amount of magnesium ions is detrimental to human osteoblasts.[36] Interestingly, our previous studies discovered that a specific range of magnesium ions (i.e., 50–100 ppm) could trigger upregulation of osteogenic genes of mouse preosteoblasts MC3T3-E1 and promote new bone formation in animals.[37–39]

PCL is an aliphatic polyester in which it can be degraded through enzymatic attack or simple hydrolysis, or both at the same time.[40] The degradation can be divided into two stages. The first stage involves the decrease of molecular weight without the loss of mass and structural deformation.[41] During the second stage degradation, PCL will break down into pieces and loss of mass and molecular weight can be therefore detected. Finally, PCL will be gradually absorbed and excreted by the human body.[41] The other literature suggested that homogeneous degradation happens to PCL[42] and the degradation mechanism of PCL is attributed by random hydrolytic chain scission of the ester linkages that results in decrease in molecular weight.[41] In fact, the molecular weight, film thickness, and crystallinity are the factors to control the degradation of PCL.[40] The degradation rate is reduced when the crystallinity increased.[40] Since our PCL coating is fabricated by solvent evaporation technique, the degradation mechanism is expected to be the same as the conventional PCL mentioned in the literatures. Due to the increased crystallinity after heat treatment, the degradation rate is therefore reduced. However, our in vitro immersion experiment could not demonstrate significant difference between nontreated PCL-coated group and heat-treated PCL-coated group in terms of degradation. In fact, the Dulbecco's modified Eagle medium (DMEM) or simulated body fluid (SBF) does not contain enzymes. Hence, the in vitro experiments are difficult to reflect the degradation behavior of PCL coatings under in vivo conditions, as enzymatic attack is expected under animal environment.

A prescreening process was conducted before the current heat treatment condition fixed. The heat treatment temperature was varied from 60 to 80 °C at 10 kPa for 1 h and it was found that the highest crystallinity could be obtained by 60 °C treatment. Moreover, since the melting point of PCL is ≈60 °C, the PCL coating will undergo recrystallization during the melting process. Hence, this explains why the crystallinity has been changed after the heat treatment.

Diez et al.[19] have also developed hydroxyapatite/poly-L-lactic acid double coating on magnesium substrate in order to enhance its mechanical and biological performances. Furthermore, a triple-layer NiCr/nano-yttria composite coating has

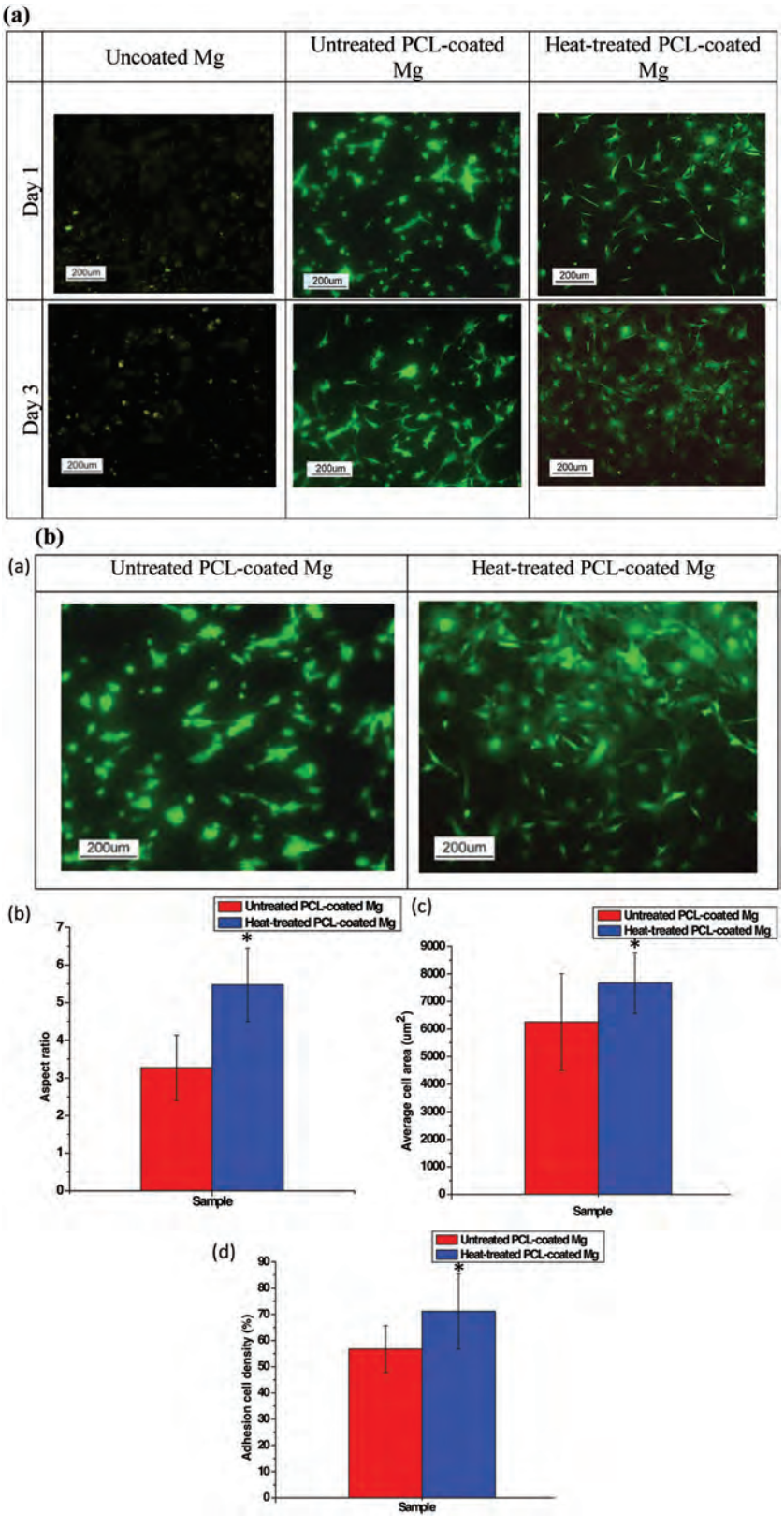

Figure 9. a) Microscopic view of the GFP mouse osteoblasts cultured on the untreated, heat-treated PCL-coated, and uncoated magnesium alloys after 1 and 3 d. 5000 GFPOB were cultured for 1 and 3 d. b) (a) Microscopic view, (b) aspect ratio, (c) average cell area, and (d) adhesion cell density of the GFP mouse osteoblasts cultured on the untreated and heat-treated PCL-coated magnesium alloys after 1 d. The aspect ratio, cell spreading area, and adhesion cell density increased significantly ($p < 0.05$) after the heat treatment.

been developed by Bakhsheshi-Rad et al.[20] for the sake of the enhancement of the corrosion and mechanical properties of Mg alloy. When compared with both coating techniques, the preparation of our coating only involves a simple and single heat treatment step that contributes to advanced biological, corrosion, and coating adhesion performance. In terms of aspect ratio, cell adhesion density, cell spreading area, as well as cell adhesion, the heat-treated PCL-coated samples are superior to both the untreated PCL-coated and uncoated samples. The water contact angle measurement also indicates that the polymer coating becomes more hydrophilic after annealing, thereby favoring cell growth on material surface.[43,44] During the heat treatment process, the samples were modified under normal atmospheric condition containing normal oxygen level. Hence, the oxygen contents of the oxygen function groups, C=O and C−O are therefore elevated.[45,46]

The literatures demonstrated that the increased hydrophilicity of polymer is attributed by the strong interaction between functional groups and water molecules.[45] Our findings revealed that the ratio of C=O and C−O of the heat-treated sample is higher than that of the control. Indeed, the C=O group is more hydrophilic than the C−O group, suggesting that the altered ratio of the C=O and C−O group not only favors cellular activity in vitro but also reinforce subsequent new bone formation in vivo.[47,48] Figure S4 (Supporting Information) shows an illustration to demonstrate the transition of molecular structure of PCL coating before and after heat treatment.

Moreover, in terms of corrosion resistance, the controlled release of magnesium ions provides a stable microenvironment on material surface, in which the suppressed release of Mg^{2+} benefits cell adhesion and proliferation in vitro, as well as bone formation under in vivo conditions. In contrast, no living cell is observed on the surface of the uncoated sample. It is believed that the continuous degradation and oxidization on the uncoated magnesium surface has created an unstable interface which is unfavorable to cell attachment.[37] The other underlying reason is possibly due to the large amount of

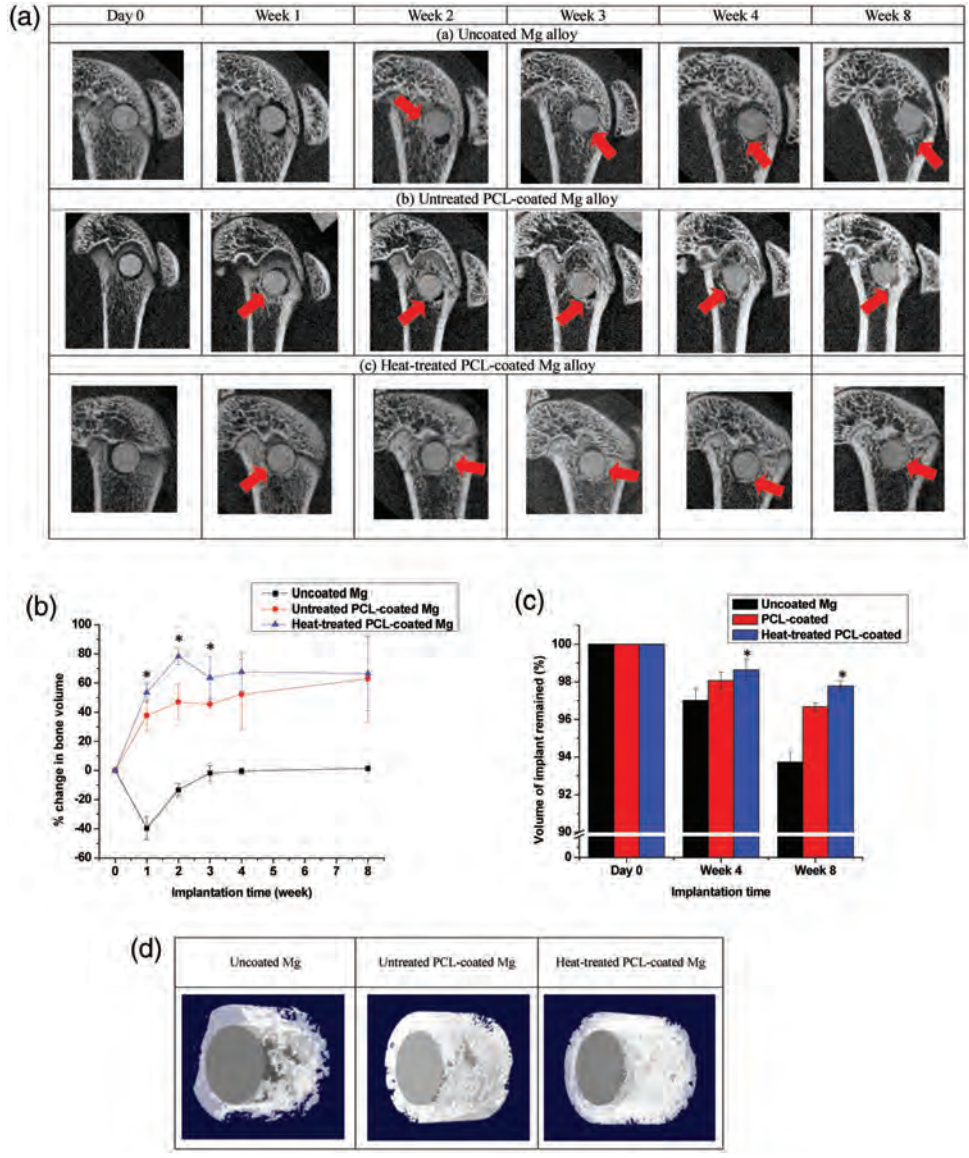

Figure 10. a) μCT reconstruction images of the lateral epicondyle containing (a) uncoated, (b) untreated PCL-coated Mg alloy, and (c) heat-treated PCL-coated Mg alloy immediately after surgery and one, two, three, four, and eight weeks postoperation. New bone formation (red arrow) can be observed progressively throughout the time points. b) Percentage changes of the bone volume around the untreated PCL-coated, heat-treated PCL-coated, and uncoated implants immediately after surgery and one, two, three, four, and eight weeks postoperation. Bone resorption was found on the uncoated sample. More than 30% and 50% of bone formation was found on the untreated PCL-coated and heat-treated PCL-coated samples after one week, respectively. c) Implant volume of the untreated PCL-coated, heat-treated PCL-coated, and uncoated implants immediately after surgery and four and eight weeks postoperation. The implant volume of the uncoated sample dropped to 97% and 93% after week 4 and week 8, respectively. The volume of the untreated and heat-treated PCL-coated implants maintained at 96% after eight weeks. d) μCT 3D reconstruction models of new bones (white color) around the implant (gray) on the uncoated, untreated PCL-coated, and heat-treated PCL-coated implants after two months postoperation.

magnesium ions released, excessive hydrogen gas generated, and the change in local pH value.[49,50]

The literatures demonstrated that the aforementioned factors could jeopardize the cell viability and subsequent new bone formation.[37] When the protective polymer membrane is present, the degradation rate of magnesium alloy is retarded and, hence, increases adhesion and proliferation as well as the differentiation capabilities of osteoblasts.[37]

In the in vivo study, the change of bone volume adjacent to the implant was qualitatively and quantitatively measured by using microcomputed tomography from day 1 until post-operation eight weeks. The amount of newly formed bone on the heat-treated samples was obviously higher among all the samples, whereas bone loss was found on the uncoated sample after one week of operation. This observation appears to be highly associated with the amount of magnesium ions released. Witte et al.[14] also reported that the bone volume adjacent to the implant could only start to increase after one week of implantation in animal model, since the uncoated magnesium alloy became stabilized due to the formation of oxide and/or

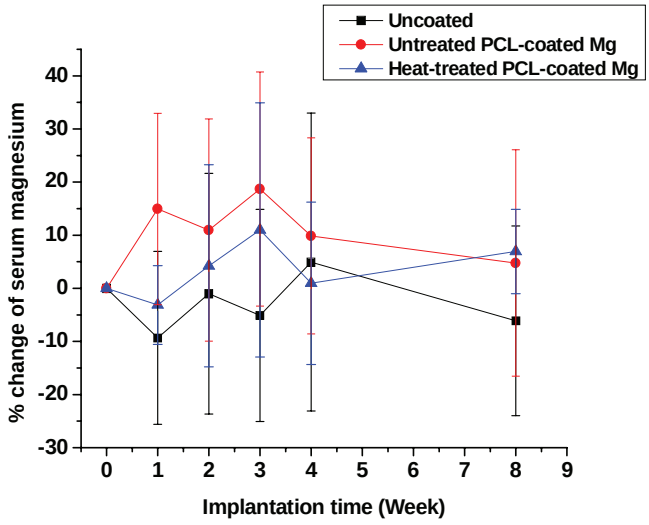

Figure 11. Percentage changes in the serum magnesium levels of the rats implanted with the untreated PCL-coated, heat-treated PCL-coated, and uncoated implants before and one, two, three, four, and eight weeks postoperation. The magnesium ion concentrations were determined by inductively coupled plasma optical emission spectroscopy (ICP-OES) after serum isolation from whole blood.

hydroxide layer on the surface of uncoated substrate after one week operation.[51] Hence, the new bone formation seems to be highly correlated to the amount of magnesium ions released.

Our previous study found that, when mouse preosteoblasts were cultured with a gradient concentration of magnesium ions, the higher Mg^{2+} concentration resulted in lower cell viability. The high Mg^{2+} concentration even downregulates the osteogenic differentiation gene expression, for example, alkaline phosphatase (ALP), osteopontin (*Opn*), type I collagen (*Col1a1*), and runt-related transcription factor (*Runx2*).[37]

In terms of histological analysis, the largest amount of new bone formation was found adjacent to the heat-treated polymer-coated implant, while less bone and fibrous tissues were observed around the uncoated implant. Surprisingly, the Young's modulus of the newly formed bone, adjacent to the heat-treated polymer-coated sample, was significantly higher than the others, suggesting that high-quality bony tissue was likely formed. We suspect that the increase of surface hydrophilicity, oxygen content, and crystallinity of polymer matrix may result in superior mineral deposition in the process of new bone formation. In fact, Kilpadi et al. mentioned that surface hydrophilicity is a factor known to alter cellular response.[52] Other research also proposed that bone apposition can be enhanced when the surface hydrophilicity is improved.[53,54]

With respect to safety concerns regarding this degradable metallic material, the magnesium ion concentrations in blood serum and internal organs, such as the liver and kidney, were measured. Our findings suggested that the serum magnesium level was within the normal physiological range.[55–57] Moreover, no degradation product adjacent to the implant was found under the examination of scanning electron microscopy and energy-dispersive X-ray spectroscopy, respectively. With respect to the release of Al of AZ91 alloy, it had been studied in vitro in our previous study.[58] The AZ91 materials were subjected to SBF immersion for 28 d. Neither Al ion nor Zn ion was detectable by using inductively coupled plasma mass spectroscopy during this period of time. Furthermore, no adverse clinical and histological effect such as prolonged tissue inflammation was found in the rats either implanted with uncoated or coated Mg samples throughout the implantation period.

Furthermore, the poor adhesion strength of polymer coating may hamper its clinical adoption.[59] The coating may delaminate from substrate surface,[60] when it is subjected to mechanical shear. A couple of studies have investigated the adhesion between PCL coating and substrate by using spin-coating

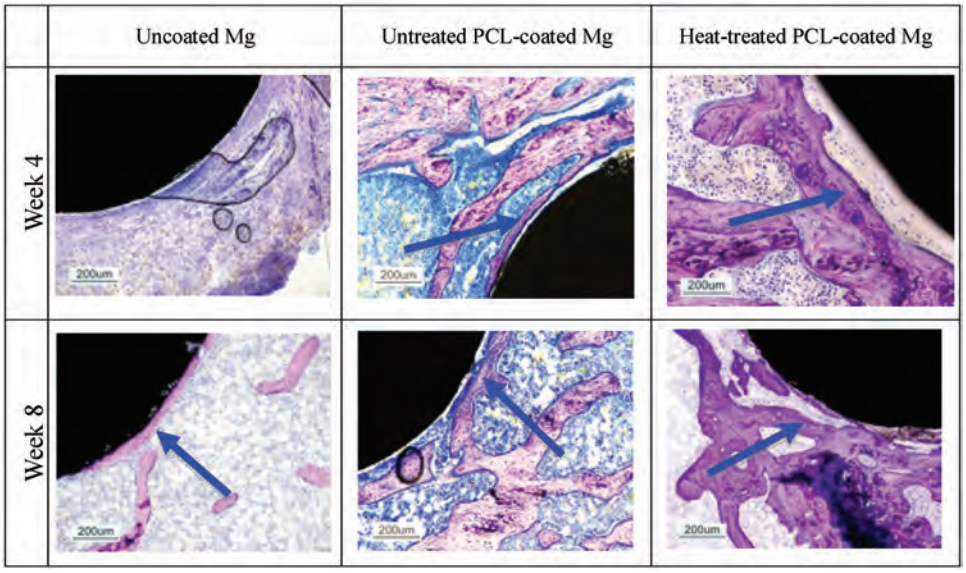

Figure 12. Histological photographs of Giemsa-stained bone tissues formed around the implant after four and eight weeks in the lateral epicondyle. Blue arrows represent the newly formed bones.

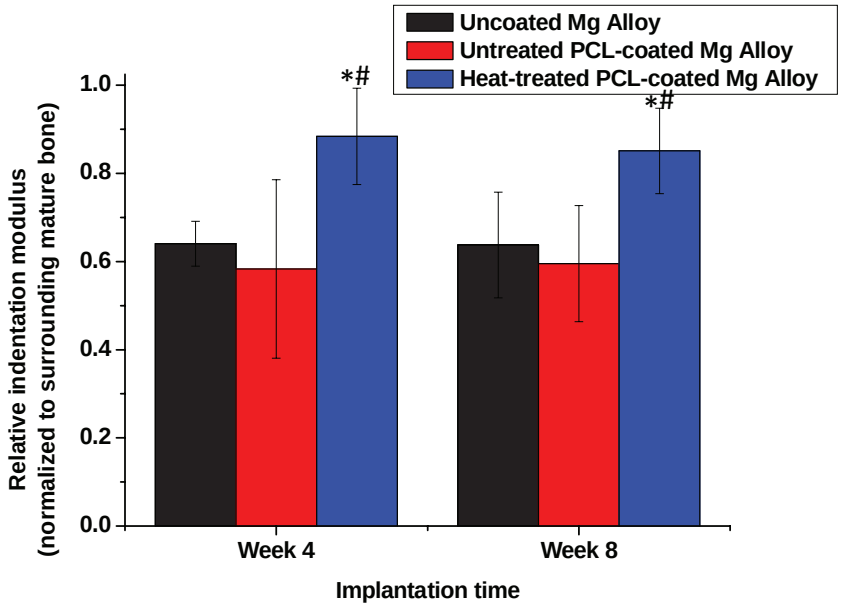

Figure 13. Relative indentation moduli of the uncoated, untreated, and heat-treated samples (normalized to nearby mature bone) at different time points. The heat-treated samples can restore ≈80% of its modulus of the nearby mature bone which is significantly higher than the untreated ($^{\#}p < 0.05$) and uncoated samples ($^{*}p < 0.05$).

technique.[32,61] In our modified peel-off testing, the adhesion strength between Mg substrate and polymer membrane was improved by the custom-designed heat treatment protocol. It is possibly because of the reorganization of polymer structure at melting temperature. As reported by Sanchez-Adsuar,[62] when the crystallinity of polymer is increased, the degree of phase separation and structure organization also increase accordingly. Hence, this change may reinforce the adhesion properties of PCL coating. In our differential scanning calorimetry (DSC) and XRD examinations, the results indicated that the crystallinity of our PCL coatings was elevated after heat treatment. Apart from the higher C=O to C—O ratio, the increased crystallinity was also attributed by the melting process of PCL coating during heating. Since the heat treatment process was carried at the temperature close to the melting point of PCL, the coating would melt and then recrystallized during cool down process. As such, this melting process would provide adequate energy to PCL molecules to overcome their energy threshold such that the PCL molecule could migrate to their crystalline position. In addition, as revealed by FTIR and XPS, the other contributing factor included the increased oxygen (O) peak intensity after heating. The higher oxygen ratio may lead to substantial electrostatic interaction between polymer membrane and metallic substrate, thereby reinforcing the interfacial adhesion strength consequently.[32,61]

4. Conclusion

A functionalized PCL membrane was deposited on magnesium alloy through a custom-designed thermal protocol in which it not only controlled the release of magnesium ions and the degradation of the substrate, but also strengthened the adhesion strength at the interface of the polymer membrane and magnesium substrate. Surprisingly, the changes in hydrophilicity and C=O to C—O ratios of the polymer membrane led to superior new bone growth and enhanced the elastic modulus of the newly formed bone. These favorable outcomes are possibly attributable to the functionalized polymer membrane and the controlled release of magnesium ions. With these promising results, it is expected that the magnesium alloy, with the functionalized PCL polymer membrane, can be applied in many orthopedic surgeries.

5. Experimental Section

Sample Preparation: AZ91 magnesium ingots, containing 9 wt% aluminum and 1 wt% zinc, were purchased from Jiaozuo City Anxin Magnesium Alloys Scientific Technology Co., Ltd., China. Square specimens with dimensions of 10 mm × 10 mm were used in the adhesion test. Disks 5 mm in diameter and 4 mm thick were prepared for the electrochemical corrosion, immersion, and in vitro biological tests. Finally, rods 3 mm in diameter and 6 mm long were used in the in vivo animal assessment. All the samples were mechanically polished to remove surface oxide and then ultrasonically cleaned with ethanol solution before membrane deposition.

PCL purchased from Sigma-Aldrich, with an average molecular weight of about 80 000 g mol^{-1}, was mixed with dichloromethane (DCM) (Fisher chemicals, England). The materials containing 3.33% (w/v) PCL were dispersed in a solvent, and the polymer membrane was deposited with the use of layer-by-layer technique using a custom spraying device equipped with airflow and temperature controls to standardize the thickness, homogeneity, and adhesiveness of the membrane. The air pressure and spraying temperature were controlled at 276 kPa and 37 °C, respectively. Spraying was performed at 50% relative humidity and 22 °C, under atmospheric pressure. After drying, the PCL-coated samples were annealed in a 60 °C vacuum oven at a pressure of 10 kPa for 1 h to produce the functionalized PCL-coated magnesium alloy.

Material Properties: Thickness: The thickness of the polymer-based membrane was determined by scanning electron microscopy (Leo 1530 FEG SEM). Before the thickness examination, a gold layer was deposited on the surface of the coated sample to distinguish between polymer membrane and the epoxy. After being embedded in epoxy, the sample was polished to expose the cross section.

Crystallinity: The crystallinity of the untreated and heat-treated polymer membrane was determined by DSC (TA Analysis, 2910 MDSC V4.4E). The testing parameters and procedures were identical as the previous publication.[63] In brief, the samples weighted 5–10 mg were used, and the melting curves were recorded starting from −20 to +80 °C. The heating rate was controlled at 10 °C min^{-1}. To reduce the possibility of incomplete melting of the polymer-based membrane, 80 °C heating temperature was chosen as the upper limit. Two independent cycles of heating and cooling were initiated in which the first cycle was able to eliminate the heat history of the polymer membrane. With the reference point of 136 J g^{-1} for 100% crystalline polycaprolactone,[64] the crystallinity degree X_c% of the polymer membrane could be therefore determined.

Chemical Composition: The untreated and heat-treated polymer membrane composition deposited on the magnesium alloys was studied by FTIR equipped with the attenuated total reflection (ATR) accessory (Equinoxss/Hyperion2000, Bruker).

Microstructure: The microstructure of the untreated and heat-treated polymer-coated samples was characterized by XRD (Philips X'pert diffractometer) with Cu Kα radiation (λ = 0.154056 nm) at room temperature.

Hydrophilicity: The hydrophilicity of the untreated and heat-treated polymer-coated samples was examined by water contact angle test measured by Ramé-Hart (USA) instrument at ambient humidity and temperature. Distilled water was chosen as the medium, and the droplet volume was 10 µL.

Atomic Concentration: The surface chemical composition of the untreated and heat-treated polymer-coated samples was determined by XPS (Physical Electronics PHI 5802) with monochromatic Al Kα radiation. The C 1s line at 284.5 eV was used as reference for the measurement of binding energies while Gaussian–Lorentzian peak-fitting model was adopted to deconvolute the S 2p spectra.

Bonding Strength: The bonding strength was determined by the modified peel-off test, according to ASTM standards B905-00 and D1876-08 for metallic and inorganic coatings, respectively. Instead of peeling off the polymer membrane at a certain angle, the membrane was pulled vertically. The pull-out force as the adhesion force was evaluated by the modified peel-off test (Figure S6, Supporting Information). The testing speed was 1 mm min^{-1}, and the study was performed on the 858.02 Mini Bionix materials testing system (MTS).

Corrosion Resistance: Electrochemical Corrosion Analysis: To measure the corrosion resistance of the uncoated (i.e., without PCL membrane coating), untreated, and heat-treated polymer-coated magnesium alloys, the electrochemical tests were therefore deployed. The samples were first embedded with the use of silicone rubber and the surface was exposed for the tests. The corrosion resistance was evaluated by using the three-electrode technique on a Zahner Zennium electrochemical workstation at 37 ± 0.5 °C and the medium used was standard SBF at pH of 7.40 (ion concentration of Na^+ 142.0, K^+ 5.0, Mg^{2+} 1.5, Ca^{2+} 2.5, Cl^- 147.8, HCO_3^- 4.2, HPO_4^{2-} 1.0, and SO_4^{2-} 0.5 × 10^{-3} M). Prior to the EIS measurement, the samples were immersed in 50 mL of SBF at 37 °C for 5 min. The data were recorded from 100 kHz to 100 mHz, with a 5 mV sinusoidal perturbing signal at the open-circuit potential. A saturated calomel electrode (SCE) and a platinum sheet served as the reference and counter electrodes, respectively. After the electrochemical test, the surface morphology of the samples was examined by scanning electron microscopy (Hitachi S-3400N SEM).

Immersion Test: To monitor the degradation and release of magnesium ions, five each of the uncoated, untreated, and heat-treated polymer-coated samples were individually immersed in sealable capsules containing 10 mL of SBF and incubated at 37 °C for two weeks. The rate of magnesium ion release, change of the pH values, and weight loss were determined at five independent time points of 1, 2, 4, 7, and 14 d by ICP-OES (Perkin Elmer, Optima 2100DV). To determine the true value of weight loss, the magnesium hydroxide corrosion product was first treated with chromic acid (200 g L^{-1} CrO_3 + 10 g L^{-1} $AgNO_3$) for 5 min.[65,66] The samples were then rinsed with distilled water and dried under vacuum condition.

In Vitro Studies: Cytocompatibility: To evaluate the cytocompatibility, standard cell culturing was performed. Six each of the uncoated, untreated, and heat-treated polymer-coated magnesium alloys were fixed on the bottom of a 96-well culture plate. A cell suspension, consisting of 1.7 × 10^4 cells cm^{-2} of the eGFPOB, was seeded on the uncoated, untreated, and heat-treated polymer-coated samples, in addition to wells without samples as the control. The cells were grown in 100 µL of the DMEM and incubated at 37 °C under 5% CO_2 and 95% air. The attachment and proliferation of cultured cells were analyzed at postculture 1 and 3 d, respectively. All the measurements were triplicated for statistical significance. The cell morphology was observed under a fluorescent microscopy with the use of a 450–490 nm incident filter (Niko ECL IPSE 80i, Japan). The fluorescence images at 510 nm were taken by digital camera (Sony DKS-ST5).

Cell Spreading: The extent of cell spreading was studied by measuring the aspect ratio and average cell area. The cell type and cell culture conditions were identical to those described in the previous section, except that only day 1 was included. To evaluate the cell adhesion properties before and after heat treatment, both the untreated and heat-treated PCL-coated samples were investigated.

In Vivo Animal Study: Surgical Procedures: 30 two-month-old female Sprague-Dawley (SD) rats, weighing between 200 and 250 g, provided by the Laboratory Animal Unit of the University of Hong Kong, were used in this study. All the handling protocols such as anesthesia, surgery, and postoperative care fulfilled the requirements set by the Ethics Committee of the University of Hong Kong and the Licensing Office of the Department of Health of the Hong Kong Government. The anesthesia of animals was induced by the intraperitoneal injection of ketamine (67 mg kg^{-1}) and xylazine (6 mg kg^{-1}). The preoperation and postoperation procedures were identical as described in previous study.[37] The uncoated, untreated, and heat-treated polymer-coated magnesium rods were implanted into the prepared holes on either the left or right femur of the rats (Figure S5, Supporting Information). The rats were sacrificed at post-op two months.

Bone Formation and Implant Degradation: In order to assess the degradation behavior of the uncoated, untreated, and heat-treated polymer-coated samples under in vivo condition and new bone formation adjacent to the implants, a set of time points at one, two, three, four, and eight weeks were scheduled. µCT (SKYSCAN 1076, Skyscan Company) scanning was employed to evaluate the volume of new bone formation and the rate of implant degradation by using CTAn program (Skyscan Company), while 3D model reconstructions were generated by using CTVol program (Skyscan Company).

Magnesium Ion Measurement: Blood samples were harvested at preoperation and postoperation one, two, three, four, and eight weeks so as to measure the concentration of magnesium ions in animal body. The processing procedure of blood samples was the same as previously described.[37] In brief, the blood samples were centrifuged and diluted to ten times with deionized water. The Mg^{2+} concentration were then determined by ICP-OES (Optical Emission Spectrometer, Perkin Elmer, Optima 2100DV). The total magnesium ions released from coated samples were compared to the uncoated controls.

Apart from the measurement of magnesium ions from blood samples, the tissue samples harvested from liver and kidneys were also assessed after euthanization. Tissue digestion protocol was performed according to a previous publication.[67] In brief, 0.2 g of liver and kidney samples were digested in the mixture of 3 mL concentrated nitric acid and 2 mL hydrogen peroxide at 85 °C hydrothermal reactor for 2 h. Then, 2% of 5 M nitric acid was added to the digested sample so as to reduce the acid effect[68] before ICP-OES analysis.

Histological and Mechanical Properties of Newly Formed Bone: The rats were euthanized at two months of postoperation, and the bone samples harvested underwent hard tissue processing as previously described.[63] The implants were fixed in 10% buffered formalin for 3 d followed by a standard tissue processing step from aqueous solution to organic one. A standardized dehydrating process from 70%, 95%, and 100% ethanol was sequentially implemented in which the samples were kept in each ethanol for 3 d. Finally, the samples were immersed into xylene for another 3 d before embedded with methyl methacrylate.[69]

There were four stages for methyl methacrylate embedding (i.e., MMA I, MMA II, MMA III, and MMA IV). The composition of each MMA solution is shown below.

MMA I solution: 60 mL of MMA (MERCK, Germany), 35 mL of butylmethacrylate (Aldrich, USA), 5 mL of methylbenzoate (Aldrich, USA), and 1.2 mL of polyethylene glycol 400 (Wako, Japan)

MMA II solution: 100 mL of MMA I and 0.4 g dry benzoyl peroxide (MERCK, Germany)

MMA III solution: 100 mL of MMA I and 0.8 g dry benzoyl peroxide (MERCK, Germany)

MMA IV solution: 400 µL of *N*,*N*-dimethyl-*p*-toluidine (Sigma, USA) and 100 mL of cold (4 °C) MMA III

The MMA solutions were continuously stirred for at least 1 h before application. The embedded samples were trimmed into slice with a thickness of 200 µm and then ground to a thickness of ≈50–70 µm. Giemsa (MERCK, Germany) stain was applied. The bone on-growth

and integration with the host tissue were observed under an optical microscope. The mechanical properties of the new bone formed on the uncoated, untreated, and heat-treated polymer-coated samples postoperative four and eight weeks were determined by nanoindentation (Nano Indenter G200) with the use of the sections. The maximum load of each indentation was 10 mN and the drift rate was 1.2 nm s^{-1}. Five indentations on each sample were measured and five identical samples were prepared on each group for statistical significance. In order to minimize the sample variation, the age, weight, and sex of animals used were fixed and the quantity of animals used was five in each group for statistical significance.

Statistical Analysis: The data collected from the in vitro and in vivo studies were analyzed by one-way ANOVA and expressed as means ± standard deviations. All the characterizations, mechanical tests, and in vitro experiments were triplicated. A p-value < 0.05 was considered to be statistically significant.

Supporting Information

Supporting Information is available from the Wiley Online Library or from the author.

Acknowledgements

H.M.W. and Y.Z. contributed equally to this work. This study was financially supported by the AO Trauma Research Grant 2012, Hong Kong Research Grant Council General Research Funds (RGC GRF) (Nos. 718913, 772113, 17214516, and 112212), City University of Hong Kong Strategic Research Grant (SRG) No. 7004188, HKU Seeding Fund (Nos. 201309176106 and 201411159045), Hong Kong Innovation Technology Fund (No. ITS/147/15), Hong Kong Health and Medical Research Fund (No. 03142446), National Natural Science Foundation of China (NSFC) (Nos. 31370957, 51422102, and 81572113), Special Prophase Program for Key Basic Research of the Ministry of Science and Technology of China (973 Program) (No. 2014CB660809), as well as Shenzhen Innovative Technology Commission Grant (Nos. JCYJ20140414090541811 and JCYJ20160429185449249).

Received: November 10, 2016
Revised: January 19, 2017
Published online: February 14, 2017

[1] M. P. Staiger, A. M. Pietak, J. Huadmai, G. Dias, *Biomaterials* **2006**, *27*, 1728.
[2] M. Niinomi, *Metall. Trans. A* **2002**, *33*, 447.
[3] J. Nagels, M. Stokdijk, P. M. Rozing, *J. Shoulder Elbow* **2003**, *12*, 35.
[4] H. Winet, J. O. Hollinger, *J. Biomed. Mater. Res.* **1993**, *27*, 667.
[5] M. Dauner, H. Planck, L. Caramaro, Y. Missirlis, E. Panagiotopoulos, *J. Mater. Sci.: Mater. Med* **1998**, *9*, 173.
[6] D. C. Tunc, W. B. Lehmann, A. Strongwater, F. Kummer, *Trans. Annu. Meet. Soc. Biomater.* **1985**, *8*, 214.
[7] A. S. Litsky, *J. Appl. Biomater.* **1993**, *4*, 109.
[8] G. Song, S. Song, *Adv. Eng. Mater.* **2007**, *9*, 298.
[9] W. Barfield, G. Colbath, J. DesJardins, Y. An, L. Hartsock, *Curr. Orthop. Pract.* **2012**, *23*, 146.
[10] E. McBride, *J. Am. Med. Assoc.* **1938**, *111*, 2464.
[11] J. Verbrugge, *La Press Med.* **1934**, *23*, 460.
[12] J. E. Gray, B. Luan, *J. Alloys Compd.* **2002**, *336*, 88.
[13] A. Yamamoto, A. Watanabe, K. Sugahara, H. Tsubakino, S. Fukumoto, *Scr. Mater.* **2001**, *44*, 1039.
[14] F. Witte, V. Kaese, H. Haferkamp, E. Switzer, A. Meyer-Lindenberg, C. J. Wirth, H. Windhagen, *Biomaterials* **2005**, *26*, 3557.
[15] V. Troitskskii, D. Tsitrin, *Khirurgiia* **1944**, *8*, 60.
[16] S. Shadanbaz, J. Walker, T. B. F. Woodfield, M. P. Staiger, G. J. Dias, *J. Mater. Sci.: Mater. Med.* **2014**, *25*, 173.
[17] G. Y. Liu, S. Tang, D. Li, J. Hu, *Corros. Sci.* **2014**, *79*, 206.
[18] T. S. N. S. Narayanan, I. S. Park, M. H. Lee, *Prog. Mater. Sci.* **2014**, *60*, 1.
[19] M. Diez, M. H. Kang, S. M. Kim, H. E. Kim, J. Song, *J. Mater. Sci.: Mater. Med.* **2016**, *27*, 34.
[20] H. R. Bakhsheshi-Rad, E. Hamzah, A. F. Ismail, M. Daroonparvar, M. A. M. Yajid, M. Medraj, *J. Alloys Compd.* **2016**, *658*, 440.
[21] J. A. Pena, S. J. Gutierrez, J. C. Villamil, N. A. Agudelo, L. D. Perez, *Mater. Sci. Eng., C* **2016**, *58*, 60.
[22] D. W. Hutmacher, M. A. Woodruff, *Prog. Polym. Sci.* **2010**, *35*, 1217.
[23] M. Domingos, F. Intranuovo, A. Gloria, R. Gristina, L. Ambrosio, P. J. Bartolo, P. Favia, *Acta Biomater.* **2013**, *9*, 5997.
[24] E. D. Yildirim, D. Pappas, S. Guceri, W. Sun, *Plasma Processes Polym.* **2011**, *8*, 256.
[25] H. Lee, G. Kim, *J. Mater. Chem.* **2011**, *21*, 6305.
[26] H. Seyednejad, D. Gawlitta, W. J. A. Dhert, C. F. Van Nostrum, T. Vermonden, W. E. Hennink, *Acta Biomater.* **2011**, *7*, 1999.
[27] M. H. Huang, S. M. Li, D. W. Hutmacher, J. T. Schantz, C. A. Vacanti, C. Braud, M. Vert, *J. Biomed. Mater. Res. A* **2004**, *69A*, 417.
[28] P. Molitor, V. Barron, T. Young, *Int. J. Adhes. Adhes.* **2001**, *21*, 129.
[29] T. Moskalewicz, S. Seuss, A. R. Boccaccini, *Appl. Surf. Sci.* **2013**, *273*, 62.
[30] S. Rahoui, V. Turq, J. P. Bonino, *Surf. Coat. Technol.* **2013**, *235*, 15.
[31] T. Elzein, M. Nasser-Eddine, C. Delaite, S. Bistac, P. Dumas, *J. Colloid Interface Sci.* **2004**, *273*, 381.
[32] J. Degner, F. Singer, L. Cordero, A. R. Boccaccini, S. Virtanen, *Appl. Surf. Sci.* **2013**, *282*, 264.
[33] M. M. Mirhosseini, V. Haddadi-Asl, S. S. Zargarian, *J. Appl. Polym. Sci.* **2016**, *133*, 43345.
[34] D. Walsh, T. Furuzono, J. Tanaka, *Biomaterials* **2001**, *22*, 1205.
[35] M. Badar, H. Lunsdorf, F. Evertz, M. I. Rahim, B. Glasmacher, H. Hauser, P. P. Mueller, *Acta Biomater.* **2013**, *9*, 7580.
[36] M. Leidi, F. Dellera, M. Mariotti, J. A. M. Maier, *Magnesium Res.* **2011**, *24*, 1.
[37] H. M. Wong, S. Wu, P. K. Chu, S. H. Cheng, K. D. Luk, K. M. Cheung, K. W. Yeung, *Biomaterials* **2013**, *34*, 7016.
[38] G. Song, *Corros. Sci.* **2007**, *49*, 1696.
[39] A. R. Boccaccini, A. Hoppe, N. S. Guldal, *Biomaterials* **2011**, *32*, 2757.
[40] V. K. Khatiwala, N. Shekhar, S. Aggarwal, U. K. Mandal, *J. Polym. Environ.* **2008**, *16*, 61.
[41] H. Sun, L. Mei, C. Song, X. Cui, P. Wang, *Biomaterials* **2006**, *27*, 1735.
[42] D. R. Chen, J. Z. Bei, S. G. Wang, *Polym. Degrad. Stab.* **2000**, *67*, 455.
[43] Z. X. Meng, Y. S. Wang, C. Ma, W. Zheng, L. Li, Y. F. Zheng, *Mater. Sci. Eng., C* **2010**, *30*, 1204.
[44] M. Parizek, N. S. Kasalkova, L. Bacakova, Z. Svindrych, P. Slepicka, M. Bacakova, V. Lisa, V. Svorcik, *Biomed. Res. Int.* **2013**.
[45] K. Moraczewski, M. Stepczynska, R. Malinowski, P. Rytlewski, B. Jagodzinski, M. Zenkiewicz, *Appl. Surf. Sci.* **2016**, *377*, 228.
[46] Z. H. Kelishomi, B. Goliaei, H. Mandavi, A. Nikoofar, M. Rahimi, A. A. Moosavi-Movahedi, F. Mamashli, B. Bigdeli, *Food Chem.* **2016**, *196*, 897.
[47] J. N. Lai, B. Sunderland, J. M. Xue, S. Yan, W. J. Zhao, M. Folkard, B. D. Michael, Y. G. Wang, *Appl. Surf. Sci.* **2006**, *252*, 3375.
[48] U. Little, F. Buchanan, E. Harkin-Jones, B. Graham, B. Fox, A. Boyd, B. Meenan, G. Dickson, *Acta Biomater.* **2009**, *5*, 2025.
[49] P. Salunke, V. Shanov, F. Witte, *Mater. Sci. Eng. B* **2011**, *176*, 1711.
[50] L. Weng, T. J. Webster, *Int. J. Nanomed.* **2013**, *8*, 1773.
[51] G. L. Song, A. Atrens, *Adv. Eng. Mater.* **1999**, *1*, 11.
[52] D. V. Kilpadi, J. E. Lemons, *J. Biomed. Mater. Res.* **1994**, *28*, 1419.

[53] D. Buser, N. Broggini, M. Wieland, R. K. Schenk, A. J. Denzer, D. L. Cochran, B. Hoffmann, A. Lussi, S. G. Steinemann, *J. Dent. Res.* **2004**, *83*, 529.
[54] T. Sawase, R. Jimbo, K. Baba, Y. Shibata, T. Ikeda, M. Atsuta, *Clin. Oral Implants Res.* **2008**, *19*, 491.
[55] N. E. L. Saris, E. Mervaala, H. Karppanen, J. A. Khawaja, A. Lewenstam, *Clin. Chim. Acta* **2000**, *294*, 1.
[56] J. Pybus, *Clin. Chim. Acta* **1968**, *23*, 309.
[57] R. Rettig, S. Virtanen, *J. Biomed. Mater. Res.* **2009**, *88A*, 359.
[58] H. M. Wong, Y. Zhao, V. Tam, S. Wu, P. K. Chu, Y. F Zheng, M. K. T. To, F. K. L. Leung, K. D. K. Luk, K. M. C. Cheung, *Biomaterials* **2013**, *34*, 9863.
[59] J. Denger, F. Singer, L. Cordero, A. R. Boccaccini, S. Virtanen, *Appl. Surf. Sci.* **2013**, *282*, 264.
[60] M. Burke, B. Clarke, Y. Rochev, A. Gorelov, W. Carroll, *J. Mater. Sci.: Mater. Med.* **2008**, *19*, 1971.
[61] L. P. Xu, A. Yamamoto, *Colloids Surf., B* **2012**, *93*, 67.
[62] M. S. Sanchez-Adsuar, *Int. J. Adhes. Adhes.* **2000**, *20*, 291.
[63] K. M. C. Cheung, H. M. Wong, K. W. K. Yeung, K. O. Lam, V. Tam, P. K. Chu, K. D. K. Luk, *Biomaterials* **2010**, *31*, 2084.
[64] T. K. Kwei, *J. Polym. Sci., Polym. Lett. Ed.* **1984**, *22*, 307.
[65] F. Witte, F. Feyerabend, P. Maier, J. Fischer, M. Stormer, C. Blawert, C. Dietael, *Biomaterials* **2007**, *28*, 2163.
[66] C. Liu, Y. Xin, G. Tang, P. K. Chu, *Mater. Sci. Eng., A* **2007**, *456*, 350.
[67] B. M. Peake, S. Ashoka, G. Bremner, K. J. Hageman, M. R. Reid, *Anal. Chim. Acta* **2009**, *653*, 191.
[68] F. Cubadda, A. Raggi, E. Coni, *Anal. Bioanal. Chem.* **2006**, *384*, 887.
[69] R. G. Erben, *J. Histochem. Cytochem.* **1997**, *45*, 307.

ADVANCED HEALTHCARE MATERIALS

Supporting Information

for *Adv. Healthcare Mater.*, DOI: 10.1002/adhm.201601269

Functionalized Polymeric Membrane with Enhanced Mechanical and Biological Properties to Control the Degradation of Magnesium Alloy

Hoi Man Wong, Ying Zhao, Frankie K. L. Leung, Tingfei Xi, Zhixiong Zhang, Yufeng Zheng, Shuilin Wu, Keith D. K. Luk, Kenneth M. C. Cheung, Paul K. Chu, and Kelvin W. K. Yeung**

Supporting Information

Functionalized Polymeric Membrane with Enhanced Mechanical and Biological Properties to Control the Degradation of Magnesium Alloy

Hoi Man Wong[a,1], Ying Zhao[a,b,d,1], Frankie K. L. Leung[a,c], Tingfei Xi[e], Zhixiong Zhang[e], Yufeng Zheng[e], Shuilin Wu[f], Keith D.K. Luk[a], Kenneth M.C. Cheung[a], Paul K. Chu[b*] , Kelvin W. K. Yeung[a,c*]

[a] Department of Orthopaedics and Traumatology, The University of Hong Kong, Pokfulam, Hong Kong, China

[b] Department of Physics and Materials Science, City University of Hong Kong, Tat Chee Avenue, Kowloon, Hong Kong, China

[c] Shenzhen Key Laboratory for Innovative Technology in Orthopaedic Trauma, The University of Hong Kong Shenzhen Hospital, 1 Haiyuan 1st Road, Futian District, Shenzhen, China

[d] Center for Human Tissues and Organs Degeneration, Shenzhen Institutes of Advanced Technology, Chinese Academy of Sciences, Shenzhen 518055, China

[e] Center for Biomedical Materials and Tissue Engineering, Academy for Advanced Interdisciplinary Studies, Peking University, Beijing 100871, China

[f] Hubei Collaborative Innovation Center for Advanced Organic Chemical Materials, Ministry-of-Education Key Laboratory for the Green Preparation and Application of Functional Materials, Hubei Province Key Laboratory of Industrial Biotechnology, Faculty of Materials Science and Engineering, Hubei University, Wuhan, China.

[1] Authors share co-first authorship

* Corresponding authors:

Dr. Kelvin W. K. Yeung: Tel: +852 22554654; Fax: +852 28174392; E-mail: wkkyeung@hku.hk

Prof. Paul K. Chu: Tel: +852 34427724, Fax: +852 34420538; E-mail: paul.chu@cityu.edu.hk

Figure S1

Mg ion concentrations in (a) kidney and (b) liver after 8 weeks of implantation. The magnesium ion concentration was determined by inductively-coupled plasma optical emission spectroscopy (ICP-OES). No significant difference was found between the uncoated and heat-treated PCL coated samples.

(a)

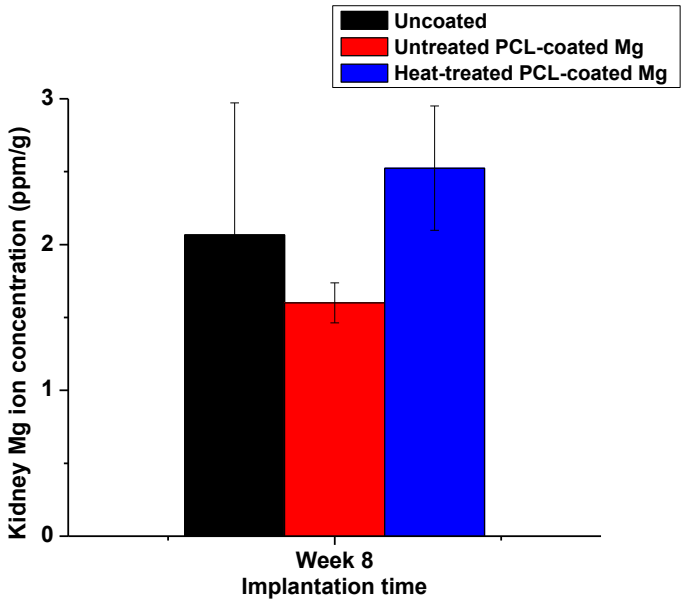

(b)

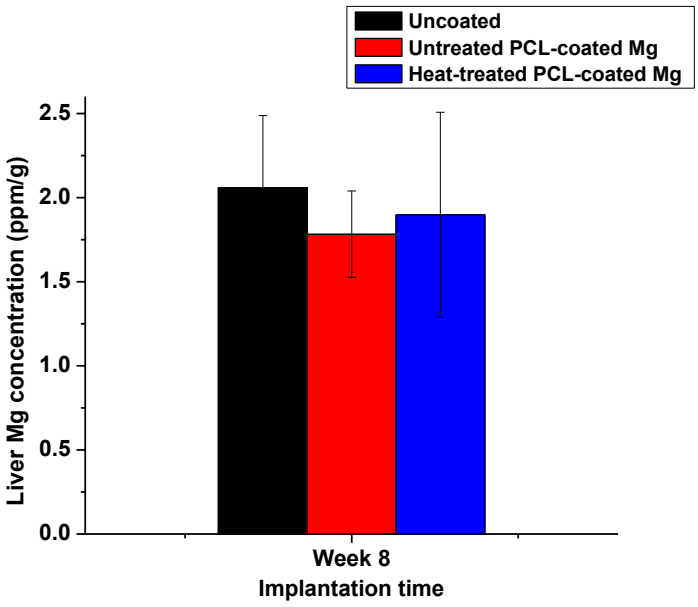

Figure S2

Interfacial morphology of the uncoated, untreated, and heat-treated samples after 4 and 8 weeks of operation under scanning electron microscopy. Corrosion was obviously found (blue arrows) on the uncoated samples in both week 4 and 8, as compared to the untreated and heat-treated samples.

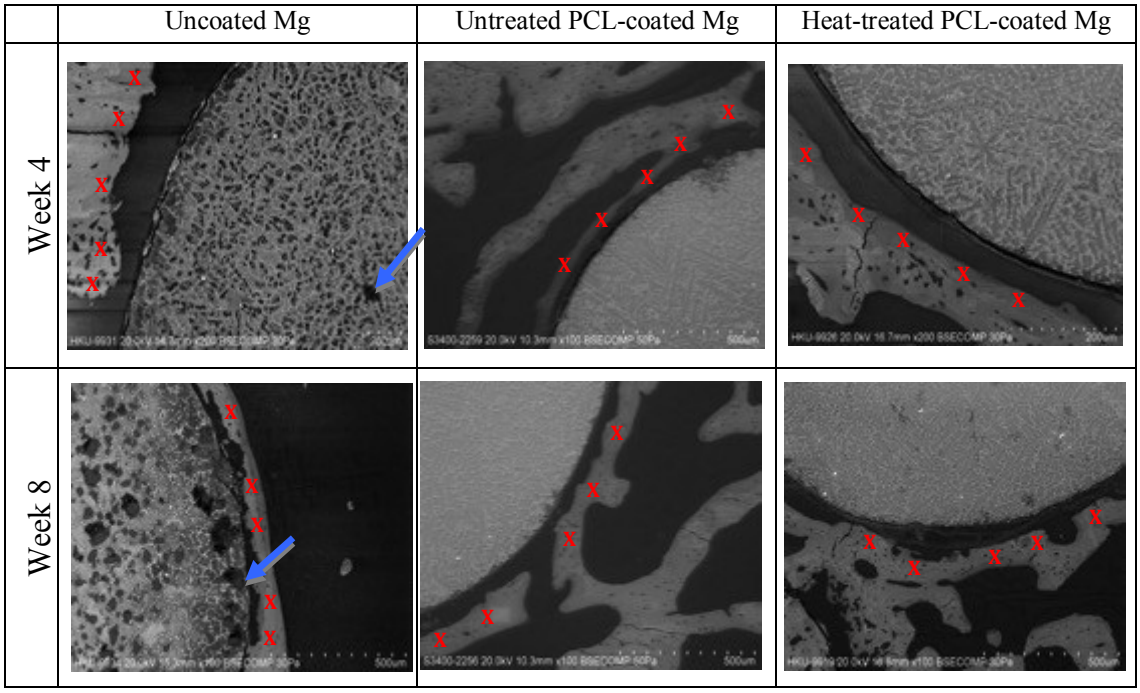

Figure S3

Load-Displacement curves of the uncoated, untreated, and heat-treated samples after 8 weeks.

Uncoated Mg	Untreated PCL-coated Mg
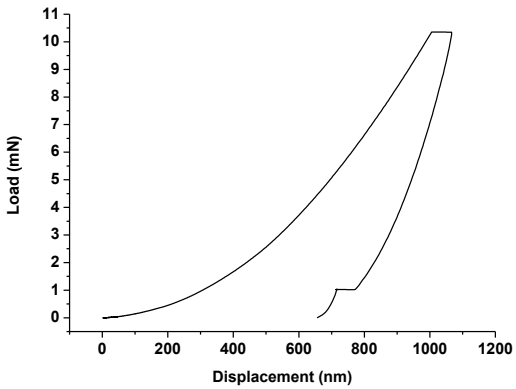	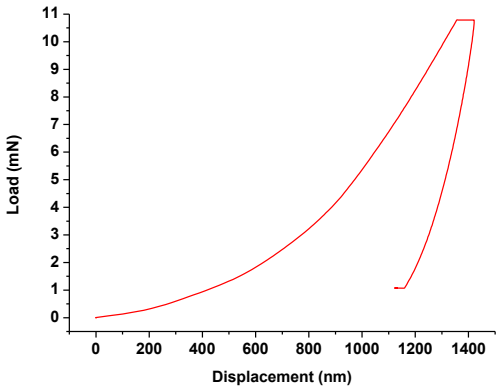
Heat-treated PCL-coated Mg	
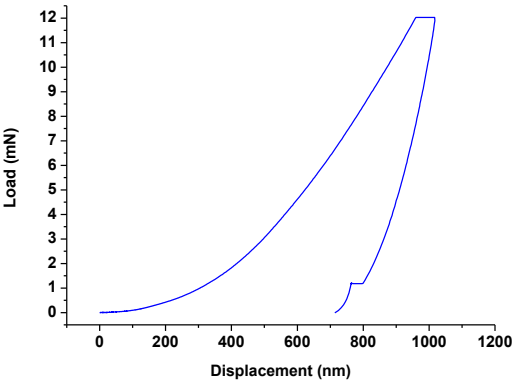	

Figure S4

An illustration to demonstrate the transition of molecular structure before and after heat treatment. Higher ratio of C=O to C-O and crystallinity were found after heat treatment. The color change of the PCL coating from light blue to dark blue represented the change of the crystallinity.

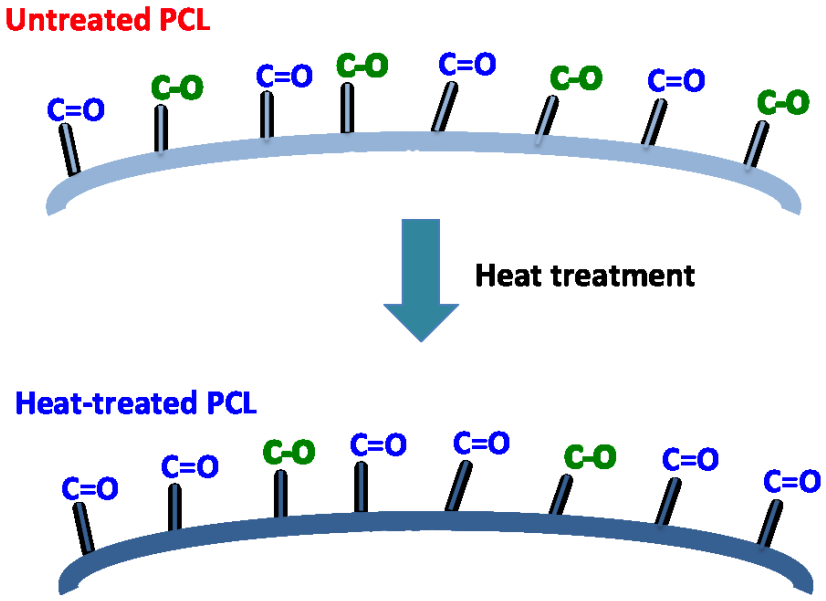

Figure S5

Surgical implantation of sample into the lateral epicondyle of SD rat after rat after two months. Black arrow shows the surgical location

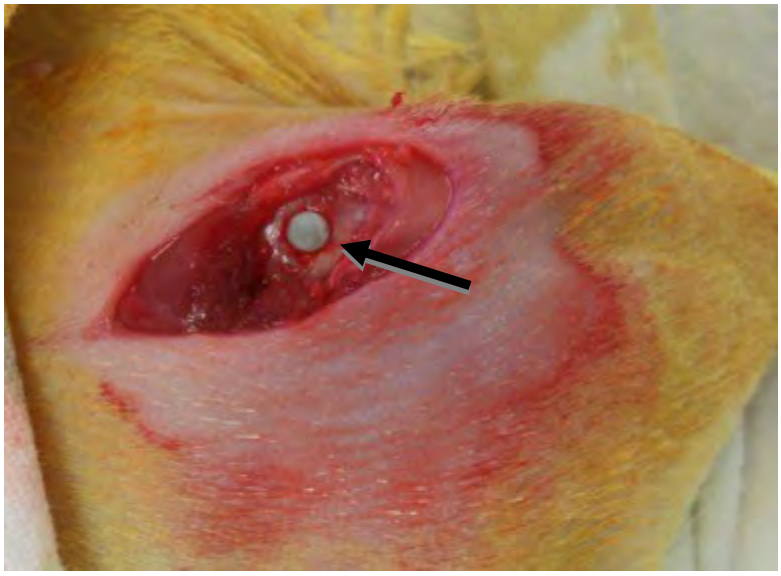

Figure S6

Schematic of the modified peel-off test apparatus